Modeling of Quench in the ITER Poloidal Field Coils

Modeling of Quench in the ITER Poloidal Field Coils

L. Cavallucci, A. Louzguiti, C. Hoa, K. Jacek, L. Junjun, P. Bauer, M. Breschi, A. Vostner

***Abstract*—The *SuperMagnet* suite of code is here applied to study the Poloidal Field (PF) and Correction Coils (CC) and their cryogenic distribution during a quench in the PF coils. In the model, more than 65 km of conductors, bus-bars, 3 km of pipes, the cold circulator, several bypass and control valves are implemented to reproduce the cryogenic circuits. The quench is simulated with an external heat disturbance at the location characterized by the lowest temperature margin during the plasma scenario. Two different approaches have been followed. In the first approach, the coils are initially assumed at their nominal conditions in "cold" state (4.4 K), before the beginning of the operating cycle. In the second approach, the initial conditions of the quench simulation correspond to those obtained in the time instant at which the lowest temperature margin is found during the plasma scenario. The main parameters to be set for the intervention of the quench protection system (threshold voltage and validation time) are finally discussed.**

***Index Terms* — Quench, Plasma Scenario, NbTi, Poloidal Field Coils, ITER project, SuperMagnet.**

I. Introduction

In superconducting fusion magnets several loss sources – such as AC losses, neutron energy deposition, heat from supports and structures – can affect the thermal stability during the plasma scenario [1-4]. In the ITER machine, the Poloidal Field (PF) Coils [5, 6] and the Correction Coils (CC) [7, 8] are part of the same cryogenic loop [9]. A quench event in one of these coils can thus affect the performance of the entire loop [10, 11]. An accurate modelling of quench is important to determine the parameters of the quench protection system, such as voltage threshold and holding time, able to prevent a permanent damage of the magnet during the quench and the following discharge.

The PF coil system consists of 6 coils wound with a NbTi Cable in Conduit Conductors (CICC) in the double pancake configuration [5]. The two-in-hand winding scheme is adopted for the PF coil. Two conductors (in-hand #1 and #2) are wound together to form the pancake and are connected at the joint located on the outer part of the double-pancake [5]. The two "hands" are electrically connected in series while the coolant flows in parallel in the two conductors with independent inlets and outlets.

The thermal-hydraulic analysis of the PF and CC during the 15 MA dynamic (DINA) plasma scenario with the *SuperMagnet* code [12] indicates the most critical location of the magnet during its working cycle [13]. In this work, the evolution of the temperature margin in the conductor is investigated for all turns of all coils and a minimum value of 1.65 K was observed at t = 308 s during the plasma burn at the outlet (x = 349 m) of the top pancake #18, in-hand #1, of the PF6 coil [13]. This value is above the prescribed threshold of 1.5 K for the PF conductors [14]. This critical position is characterized by the lowest minimum quench energy (MQE) and the highest quench probability during the plasma scenario.

In this work, the *SuperMagnet* code is applied to analyze the PF and CC cryogenic loop during quench events occurring at the most critical location of PF coils. The quench is investigated at the outer turn of PF6 top pancake (#18) at two different instants (see Fig. 1):

- t = 0 s, i.e. at the start of plasma discharge (SOD), without AC losses and nuclear heating in the winding pack and with the coils in a "cold state" (temperature of 4.4 K). This instant is selected because it marks the initiation of coil energization and the onset of current flow, even though the outer turn of the PF6 top pancake does not exhibit the lowest temperature margin at t = 0 s.
- t = 308 s, i.e. during the plasma burn accounting for the heat load in the winding pack derived from the scenario. This instant is selected as the temperature margin reaches its minimum in the mentioned position.

In case a quench is detected, the intervention of the quench protection system is simulated by discharging the magnet with a time constant of 14 s [15]. The current in the PF exhibits an ideally exponential profile during the discharge. The mutual coupling between the coils and the variation of the dump resistance with temperature is assumed negligible.

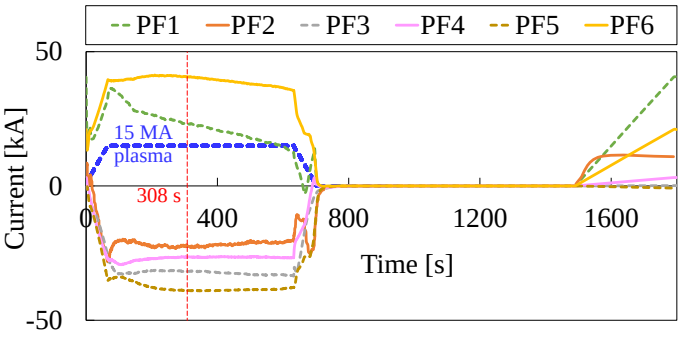

Fig. 1. Current in the PF coils during the 15 MA plasma scenario and time instants selected for the quench disturbance: t = 0 s and t = 308 s.

M. Breschi and L. Cavallucci are with the Department of Electrical, Electronic and Information Engineering, Università di Bologna, Italy *(corresponding author: lorenzo.cavallucci3@unibo.it)*.

A. Louzguiti, K. Jacek, C. Hoa, L. Junjun, P. Bauer and A. Vostner are with the ITER Organization, Cadarache, France.

The work at Università di Bologna was supported by the ITER Organization under contract # IO/ 20/CT/4300002342.

Disclaimer: The views and opinions expressed herein do not necessarily reflect those of the ITER Organization or of the European Commission.

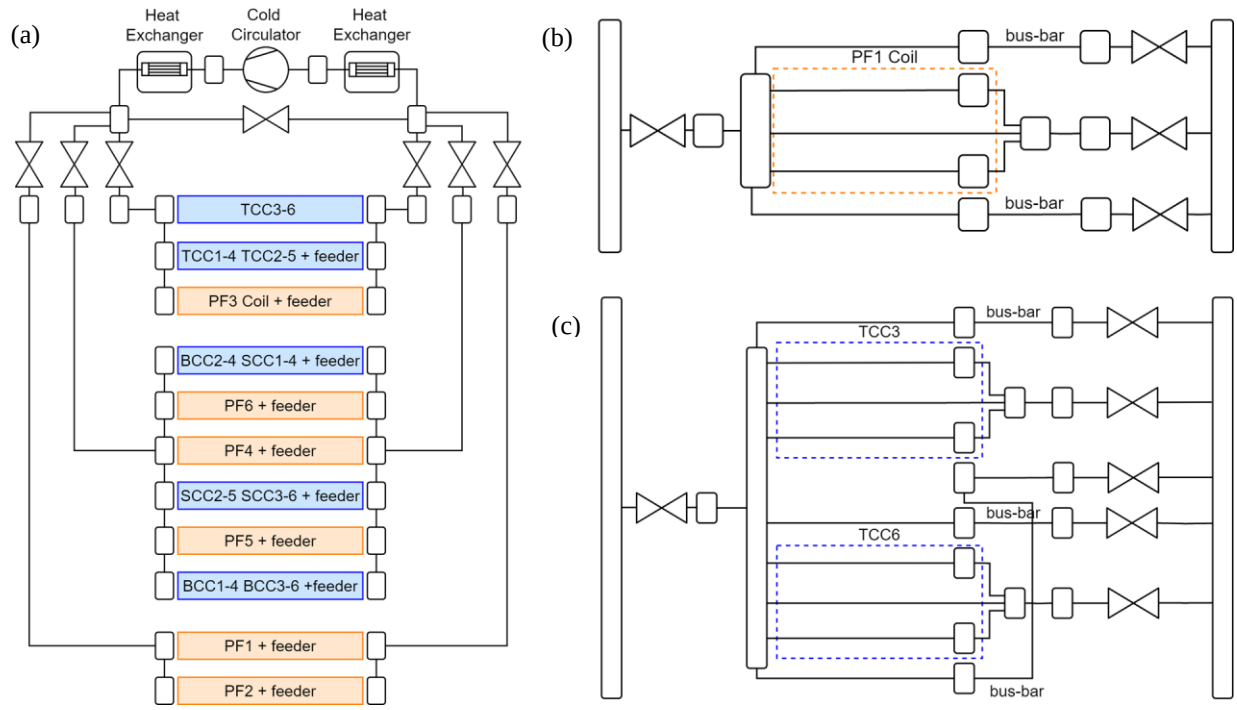

Fig. 2: (a) Cryogenic loop; (b) PF1 coil (dashed rectangle), feeder and joint locations; (c) TCC3 and 6 (dashed rectangle), feeder and joint locations;

II. Model Description

The *SuperMagnet* model [16, 17] of the PF&CC cryogenic loop is able to analyze the 6 PF coils and the Top, Bottom and Side Correction Coils. The model is also comprehensive of the feeders with the details of the cryogenic circuit described through several sub-models.

Model of the cryogenic loop: The hydraulic circuit is described in the *Flower* model [18] through the implementation of the piping, the cold circulator, the heat exchangers and the control and by-pass valves (see Fig. 2(a)). As an example, the hydraulic layout of PF1 and of TCC3 and 6 with their feeders are shown in Figs. 2(b) and 2(c) respectively.

Model of the winding pack: The *Thea* model [19] is a 1-D tool for the analysis of superconducting cables accounting for the heat conduction in the solid, the heat transfer in the coolant (bundle and spiral) and the electrical properties of the conductor [20]. The PF coils (with the details of the two-in-hand configuration), the top, bottom and side CC and the bus-bars are modelled in *Thea* (347 processes in total).

Heat diffusion in the PF stack: The *Heater* model [21] is a 2-D FEM model describing the heat diffusion in the PF stack (jacket, inter-turn and inter-pancake insulation). This model accounts for the transverse inter-pancakes thermal conduction. The 2-D mesh includes nine equally spaced cross sections of the stack for each PF coil.

Coupling Thea-Flower: These models are coupled at the boundaries of each pancake. Temperature and pressure at the extremities of the pipes are taken as an input for the inlet/outlet of the bundle and spiral of the conductor.

Coupling Thea-Heater: These models are coupled via several 1-D lines. The helium in connection with the jacket through these 1-D lines drives the heat exchange in azimuthal direction between the nine PF stacks. This allows to implement the PF stack as nine 2-D cross-sections rather than as a fully 3-D stack.

III. Quench Disturbance and Detection

To simulate quench in the PF6 coil, pancake #18, in-hand #1, a 3 ms heat pulse is deposited in the 20-m-long turn corresponding to x = 349 m (outlet of the layer). The heat pulse consists of 1 ms of ramp-up, 1 ms of flat-top and 1 ms of ramp-down. This heat deposition on a 20-m length is representative of a disruption disturbance derived from the plasma [14].

The resistive voltage of the double-pancake (pancakes #17 and #18) is compared to the voltage threshold set to either 100 mV or 400 mV. In the quench detection bridge, the resistive voltage measurement is performed by subtracting the voltage across one in-hand conductor to the voltage in the second in-hand since their inductive components are cancelling out (they approximately enclose the same magnetic flux) [22].

In the model only the resistive voltages are computed, as if the quench detection bridge was perfectly balanced. The nominal holding time of 2.0 s [15] is set to check whether or not the measured voltage keeps exceeding the prescribed threshold. This study is performed even artificially increasing the holding time to 4.0 s. Once the quench is triggered, the magnet is discharged with a time constant of 14.0 s [15]. The discharge is simulated with an exponential decay of both the current and the magnetic flux density. The coupling and hysteresis losses during the discharge are computed with analytical models [23-27].

TABLE I
QUENCH CONDITIONS

	B [T]	I_{op} [kA]	T [K]	MQE [J/cm$^3_{sc}$]
Start of Discharge (t = 0 s)	1.5	21	4.4	4.0
Plasma Burn (t = 308 s)	4.3	41	5.3	0.4

IV. QUENCH DURING THE START OF DISCHARGE

A MQE value (per unit volume of superconducting strands) of 4.0 J/cm$^3_{sc}$ is required to quench the coil at t = 0 s during the start of discharge of the plasma scenario. The MQE was determined by increasing or decreasing the power deposited on the conductor during the heat pulse. The magnetic flux density and the operating current in the location selected for the quench are shown in Table I. The resistive voltage and the hot spot temperature are shown in Figs. 3 and 4 respectively. The results are computed setting the voltage threshold to 100 mV and to 400 mV. A holding time of 2 s and 4 s is considered.

During the heat pulse, the temperature in the conductor exhibits a first spike related to the heat pulse profile. Simultaneously, the normal zone propagates through the conductor at a velocity of about 100 m/s. After the heat pulse, the temperature initially decreases (helium and conduction cooling) and then rises up again driven by Joule effect resulting from the resistive transition. At t = 0.1 s, the voltage exceeds the 100-mV threshold. After 2.0-s holding time, the quench protection system intervenes, and the magnet is discharged. The hot spot temperature exhibits a peak of 17 K about 10 s after the disturbance. The results have no re-markable variation with increasing the holding time to 4 s.

The threshold voltage of 400 mV is exceeded at t = 16.2 s and the magnet is discharged at t = 18.2 s. The peak voltage increases a factor of 4 (0.42 V) with respect to the 100 mV-threshold. The hot spot temperature is still limited to 35 K. A higher peak temperature of 38 K is computed when increasing the holding time to 4 s. These results are in compliance with the requirement of 150 K peak temperature on the jacket.

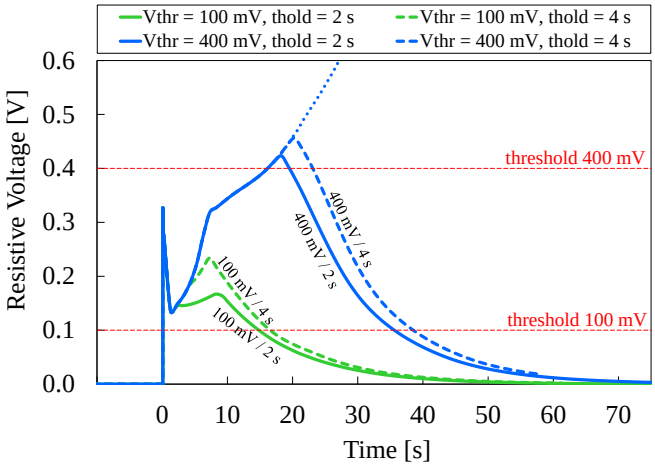

Fig. 3. Resistive voltage in the double pancake (#17 and #18) of PF6 coil during quench at the start of discharge (t = 0 s).

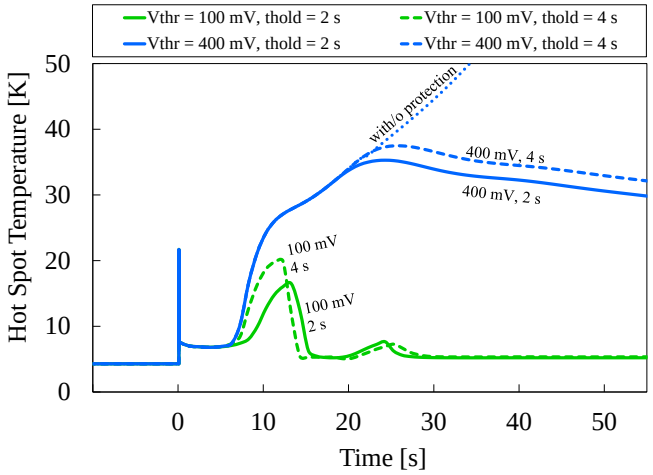

Fig. 4. Hot-spot temperature in the conductor of pancake #18 of PF6 coil during quench at the start of discharge (t = 0 s).

V. QUENCH DURING THE PLASMA BURN

The MQE required to quench the coil during the plasma burn at t = 308 s is one order of magnitude lower than at the start of discharge (t = 0 s). During the plasma burn, a higher energy is stored in the magnet with a magnetic flux density of 4.3 T and an operating current of 41 kA (see Table I). The heat load during the plasma scenario – such as AC losses in the winding pack, nuclear heating, heat load in the pipes – are accounted for in this case [27] (see Fig. 5(a)). The conductor temperature is equal to 5.3 K before the quench disturbance. During the quench, once the protection system is triggered, the magnet is discharged. The additional heat load due to the AC losses in the conductor generated during the discharge are considered in the model. An insight of the AC losses during this transient is shown in Fig. 5(b).

During the heat pulse, the normal zone propagates at a velocity of about 30 m/s. The voltage exhibits a rapid increase, shown in Fig. 6, and after 0.3 ms from the disturbance it exceeds the threshold of 100 mV. The 400-mV threshold is instead exceeded 0.6 ms after the disturbance. Setting the voltage threshold to 100 mV or to 400 mV does not have any practical impact on the results. The value of 400 mV is selected for the following analyses.

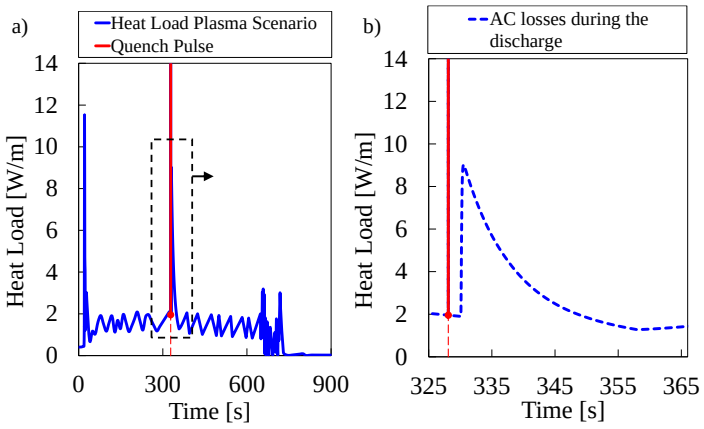

Fig. 5. a) Heat load during the plasma scenario and quench pulse at t = 308 s; b) insight between 325 s and 365 s of the AC losses in the conductor during the discharge.

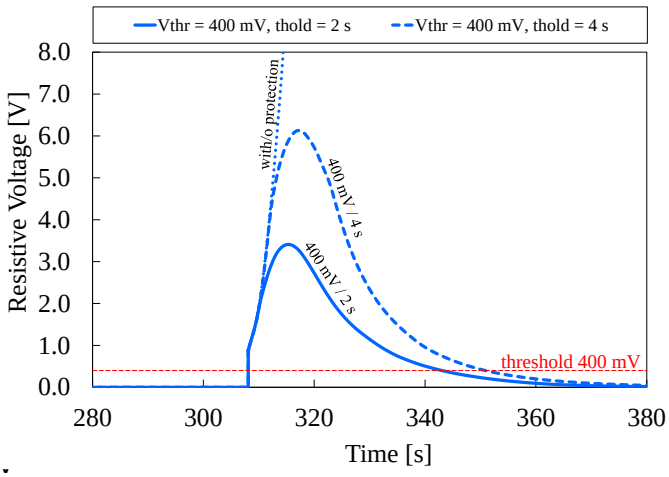

Fig. 6. Resistive voltage in the double pancake (#17 and #18) of PF6 coil during quench at the plasma burn (t = 308 s).

During quench, the resistive voltage exhibits a peak of 3.4 V with the holding time set to the nominal value of 2 s. Setting the holding time to 4 s, a peak voltage of 6.0 V is computed.

The peak temperature (not shown here) is below 50 K and 60 K, with a holding time of 2 s and 4 s respectively. The higher values of magnetic flux density and current at t = 308 s with respect to t = 0 s (see Table I) determine higher AC losses (due to the discharge) and Joule heating at t = 308 s than at t = 0 s.

In Fig. 7(a) the temperature in the jacket and in the inter-turn and inter-pancake insulations layers is shown at 0.5 s after the heat pulse. The helium back-flow rapidly propagates through the turn of the same in-hand of the quench position (in this case, the in-hand #1). The in-hand #2 is not initially affected by the quench propagation. As shown in Fig. 7(b), 1.0 s after the pulse the hot zone propagates to the in-hand #2. The transverse pancake-to-pancake heat propagation is not the driving phenomenon during quench; nonetheless its impact is not negligible.

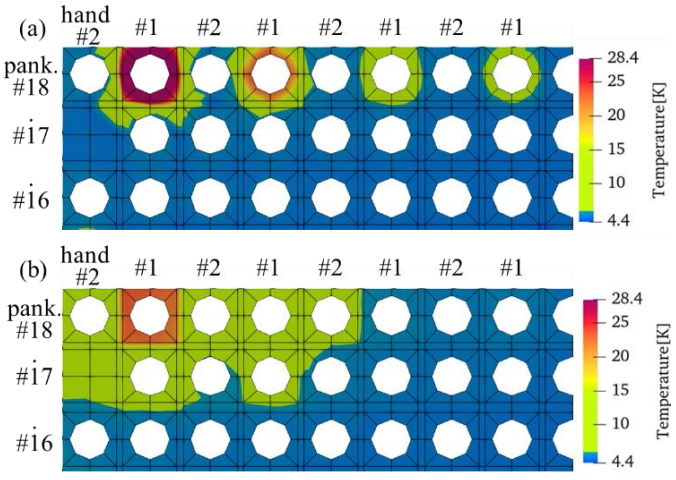

Fig. 7. Temperature in the PF stack (jacket, inter-turn and inter-pancake insulation layers) during quench at the plasma burn (t = 308 s): (a) 0.5 s after the pulse and (b) 1.0 s after the pulse.

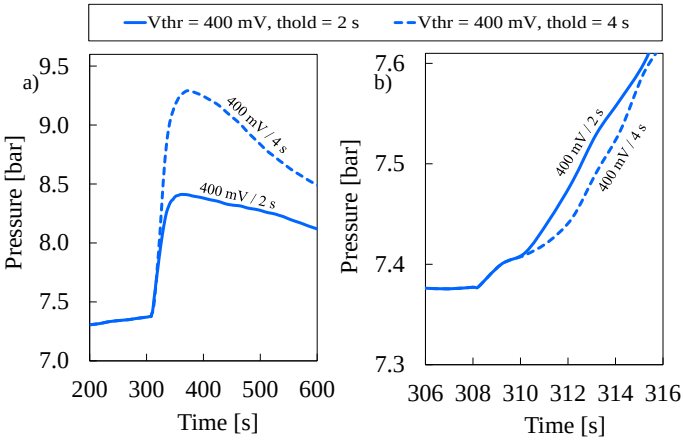

Fig. 8. (a) Pressure at the inlet manifold of the cold circulator during quench at the plasma burn (t = 308 s); (b) insight between t = 306 s and 316 s

In Fig. 8, the pressure at the inlet manifold of the cold circulator is shown during quench. The quench disturbance at t = 308 s determine a small increase of the pressure at the inlet of the circulator. In the time window between t = 310 s and t = 316 s, the pressure computed with a holding time of 4 s is lower than that with 2 s. The helium exhibits a higher pressurization during the discharge of the magnet with a bump of ΔP = 1 bar and ΔP = 2 bar with a holding time of 2 s and 4 s respectively. This pressurization is determined by the AC losses deposited during the discharge in the PF coils.

An experimental benchmark of the results here presented is not possible due to the lack of data. However, it is noteworthy that comparable pressure bumps during the discharge were observed in the test campaign of the Central Solenoid Module (CSM) [25, 28]. Similar pressure bumps can damage the circulator.

VI. Conclusion

In this work, the behavior of the PF coils and its cryogenic loop during quench is analyzed by simulating a heat disturbance in the turn corresponding to the lowest temperature margin during the plasma scenario (PF6, pancake #18, in-hand #1, last turn). The quench is investigated at different time instants corresponding to the start of the plasma discharge (t = 0 s) and during the plasma burn (t = 308 s); the latter corresponds to the lowest temperature margin.

The impact of the voltage threshold and the holding time on the performances during quench is studied setting the voltage thresholds to 100 mV and 400 mV and the holding time of 2.0 s and 4.0 s. In all cases, during the quench, the hot spot temperature remains well below the design requirement of 150 K.

Further conservative assessments of the results are required: decreasing the length of the disturbance (few centimeters) and locating it in different moments or positions such as the lowest magnetic field or at the highest temperature margin positions. These positions are in fact characterized by a higher quench energy (less probable quench) but even by a slower propagation velocity and thus by a higher hot spot temperature.

REFERENCES

[1] N. Mitchell *et al.* "The ITER magnet system," *IEEE Trans. Appl. Supercond.*, vol. 18, no. 2, pp. 435–440, 2008.

[2] R. Maekawa *et al.* "Dynamic simulation of ITER cryogenic system under D-T operation," *IOP Conf. Ser.: Mater. Sci. Eng.*, vol. 755, no. 012082B, 2020, doi: DOI 10.1088/1757-899X/755/1/012082.

[3] L. Savoldi *et al.* "The 4C code for the cryogenic circuit conductor and coil modeling in ITER," *Cryogenics* 50, pp. 167-176, 2010.

[4] R. Bonifetto *et al.* "Analysis of the Thermal-Hydraulic Effects of a Plasma Disruption on the DTT TF Magnets," *IEEE Trans. Appl. Supercond.*, vol. 32, no. 6, 2022, 4204007.

[5] Lim *et al.*, "Design of the ITER PF Coils," *IEEE Trans. Appl. Supercond.*, vol. 21, no. 3, pp. 1918-1921, June 2011, doi: 10.1109/TASC.2010.2092732.

[6] M. Liao *et al.*, "Completion and Installation of the ITER Lower Poloidal Field Coils PF5 & 6," *IEEE Trans. Appl. Supercond.*, vol. 32, no. 6, pp. 1-5, Sept. 2022, Art no. 5300105, doi: 10.1109/TASC.2022.3166128.

[7] A. Foussat *et al.*, "Overview of the ITER Correction Coils Design," *IEEE Trans. Appl. Supercond.*, vol. 20, no. 3, pp. 402-406, June 2010, doi: 10.1109/TASC.2010.2041911.

[8] P. Libeyre *et al.*, "Qualification of the Manufacturing Procedures of the ITER Correction Coils," *IEEE Trans. Appl. Supercond.*, vol. 27, no. 4, pp. 1-5, June 2017, Art no. 4201405, doi: 10.1109/TASC.2016.2630728.

[9] L. Serio *et al.* "The Cryogenic System for ITER," *Fus. Sci. and Technol.*, vol. 56, no. 2, pp. 672-675, 2008, doi: 10.13182/FST09-A8986.

[10] M. Bagnasco *et al.* "Progress in the integrated simulation of thermal-hydraulic operation of the ITER magnet system," *IEEE Trans. Appl. Supercond.*, vol. 20, no. 3, pp. 411–414, Jun. 2010.

[11] L. Cavallucci *et al. "*Multiphysics Model of Quench for the ITER Central Solenoid*", IEEE Trans. Appl. Supercond.*, vol. 33, n. 5, 2023.

[12] CryoSoft, "SuperMagnet, Multitasking code manager", User's Guide, version 2.1, February 2016.

[13] A. Louzguiti *et al.* "Updated stability analysis of the PF/CC models with the ITER DINA 2016 plasma scenario", *submitted for publication.*

[14] Magnet Superconducting and Electrical Design Criteria, internal report IDM 22GRQH, 2009.

[15] DDD11-1 System Requirements Expansion and Design Choices, internal report IDM 2NPLKM, 2016.

[16] L. Bottura *et al.* "A Numerical Model for the Simulation of Quench in the ITER Magnets", *J. Comp. Phys.*, vol. 125, no. 77, pp. 26-41, 1996.

[17] L. Bottura and C. Rosso, "Flower, a model for the analysis of hydraulic networks and processes," *Cryogenics*, vol. 43, no. 3–5, pp. 215–224, 2003.

[18] CryoSoft, "Flower, Hydraulic Network Simulation", User's Guide, version 4.5, January 2016.

[19] CryoSoft, "Thea, Thermal, Hydraulic and Electrical Analysis of Superconducting Cables", User's Guide, version 2.3, September 2016.

[20] L. Bottura *et al.* "A general Model for thermal, hydraulic and electric analysis of superconducting cables," *Cryogenics*, vol. 40, pp. 617–626, 2000.

[21] CryoSoft, "Heater, Simulation of Heat Conduction", User's Guide, version 2.1, February 2016.

[22] Principle of Quench Detection in PF, internal report IDM PJ37K3, 2014.

[23] P. Bauer *et al.*, "Description of the AC Loss Model for the ITER Central Solenoid During a Plasma Scenario", *IEEE Trans. Appl. Supercond.*, vol. 32, no. 6, 2022.

[24] A. Torre *et al.* "Review of Experimental Results and Models for AC Losses in the ITER PF and CS Conductors", *IEEE Trans. Appl. Supercond.*, vol. 32, n. 6, 2022.

[25] M. Breschi *et al.* "AC losses in the first ITER CS module tests: Experimental results and comparison to analytical models," *IEEE Trans. Appl. Supercond.*, vol. 31, no. 5, 2021, 5900905.

[26] M. Breschi *et al.* "Analysis of losses in superconducting magnets based on the Nb3Sn Rutherford cable configuration for future gantries", *Supercond. Sci. and Technol.*, vol. 31, no. 1, 2018, 015005

[27] P. Bauer *et al.*, "AC Losses Calculations for the ITER CS and PF Magnet Systems during Plasma Operation", *IEEE Trans. Appl. Supercond., vol.* 33, no. 5, 2023.

[28] M. Breschi *et al.* "AC Losses in the Second Module of the ITER Central Solenoid," *IEEE Trans. Appl. Supercond.*, vol. 32, no. 6, 2022, 4700505.